Approaching Bose-Einstein condensation of metastable neon: Over 10^9 trapped atoms

S. J. M. Kuppens, J. G. C. Tempelaars, V. P. Mogendorff, B. J. Claessens, H. C. W. Beijerinck, and E. J. D. Vredenbregt
Eindhoven University of Technology, P. O. Box 513, 5600 MB Eindhoven, The Netherlands
(Received 27 June 2001; published 15 January 2002)

We present an experimental study of the loading of a magneto-optical trap (MOT) from a brightened and slowed beam of metastable neon atoms. The unprecedented high numbers of 9×10^9 ^{20}Ne and 3×10^9 ^{22}Ne metastable atoms are trapped under unconventional trap conditions as compared to metastable helium traps, such as low intensity and small detuning. These cause the MOT to have an extraordinarily large volume on the order of 1 cm^3 and a typical peak density of 10^{10} atoms/cm^3. A simple Doppler model is discussed which explains why the optimum is found under these conditions. The model includes the seventh beam necessary for the last slowing step before loading.

DOI: 10.1103/PhysRevA.65.023410 PACS number(s): 32.80.Pj, 34.50.Rk, 03.75.Fi

I. INTRODUCTION

The successful Bose-Einstein condensation (BEC) of alkali-metal atoms [1] has stimulated several groups [2–5] to extend the range to metastable rare gas atoms, with helium and neon being the prime candidates [6,7]. These metastable atoms are distinguished from the alkalis metals by their large internal energy of 16.7 eV and 20 eV for Ne and He, respectively. This makes them particularly interesting new candidates for BEC. The internal energy can be used for efficient detection schemes providing real-time diagnostics of the phase transition [7]. The ability to count individual atoms opens a route for studying finite size effects in BEC [8] and quantum optics experiments involving the quantum statistics of a BEC. The internal energy also presents a challenge because Penning ionization leads to high inelastic collisional loss rates at relatively low densities as compared to alkali-metal atoms. However, very recently BEC of metastable helium atoms has been observed by Robert *et al.* and by Dos Santos *et al.* [9,10], which shows that this difficulty can be overcome in a spin polarized gas, as predicted by theory [6].

In our group we aim at reaching BEC with metastable neon atoms. The first step is to trap large samples of metastable neon atoms in a magneto-optical trap (MOT) [11], which can then be transferred to a magnetic trap and cooled evaporatively [1]. Evaporative cooling is greatly facilitated when the initial number of atoms is high, e.g., 10^{10} atoms. In this paper we show how such large amounts of metastable neon atoms can be trapped in a MOT.

In contrast to the case of alkali-metal atoms, a vapor cell MOT is not possible with rare gas atoms because the latter have to be electronically excited to the metastable state to make them susceptible to laser cooling. Our MOT is loaded with a brightened and slowed atom beam [12]. The axial velocity of 100 m/s of the atoms is too large for efficient capture by a MOT. Therefore we apply an extra Zeeman slower to reduce the velocity to about 10 to 20 m/s. The geometry is depicted in Fig. 1. The laser beam used for slowing intersects the MOT. Due to the relatively small initial velocity of the atoms the slower is operated at low intensity and small detuning. Hence, the scattering force from this light on atoms in the MOT is not negligible, especially because optimal operation of the MOT also turns out to be at comparable intensities and detunings. In essence, this introduces an additional laser beam to the MOT which cannot be neglected in the description of its dynamics, i.e., a seven-beam MOT is created. This seems awkward at first but nevertheless allows for a MOT containing 9×10^9 atoms, to our knowledge the largest MOT of metastable atoms reported so far. This is more than a two orders of magnitude increase since the early work on a neon MOT by Shimizu *et al.* [13].

Comparing our results to those obtained with helium we find a completely different set of operating parameters. Whereas in helium MOTs [4,14–17] generally very large intensities and detunings are used, we trap our maximum number of atoms at very low intensity and relatively small detunings.

This paper is organized as follows. We start in Sec. II with a description of our setup. In Sec. III a model focusing on the number of atoms in our MOT is developed taking into account the Zeeman slower laser beam. Section IV contains an overview of the diagnostics that are applied to characterize

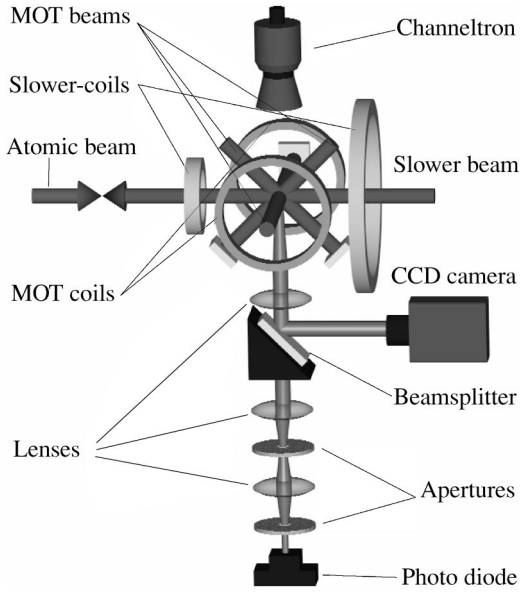

FIG. 1. Overview of the MOT and Zeeman slower including the detection setup. The probe laser beam used for absorption imaging propagates along the *z* axis and is not shown in this figure.

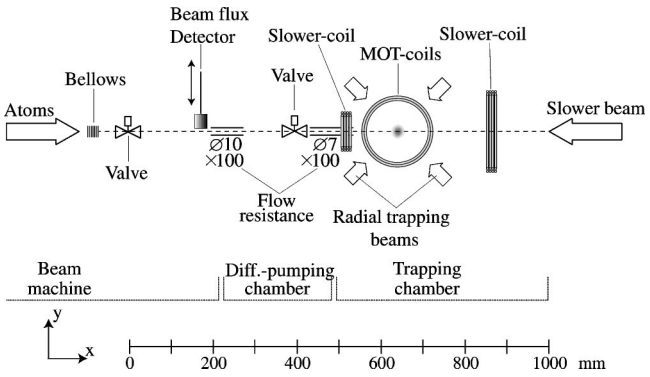

FIG. 2. Schematic side view of the trapping chamber.

the MOT. In Sec. V we present supporting data for the main features of our seven-beam MOT model. Section VI addresses the maximization of the number of trapped atoms. In Sec. VII the trap loading and loss dynamics are investigated, yielding Penning ionization rate constants resulting in a refinement of the model. In Sec. VIII we discuss the prospects of achieving BEC in our setup. We end in Sec. IX with concluding remarks.

II. EXPERIMENTAL SETUP

A. Trapping chamber

Our MOT is loaded from a bright and cold beam of metastable neon atoms [12]. Starting with a liquid-nitrogen-cooled supersonic discharge source, this beam is prepared by applying laser cooling techniques such as Zeeman slowing, Doppler cooling and collimation, and magneto-optical compression. The atom beam has a diameter of about 1 mm and the atom flux is about 3×10^{10} atoms/s. This is a pure beam of $^3P_2$ atoms. A combination of a beam stop close to the source and a small exit orifice ensures that there are no UV photons, ground state atoms, or thermal atoms in the wrong metastable state nor other isotope atoms reaching the trapping chamber. The axial velocity of the atoms is 100 m/s and the transverse velocity spread is Doppler limited.

At the exit of this beam preparation stage the vacuum pressure is 10^{-8} mbar. With BEC in mind we have inserted an additional differential pumping stage (see Fig. 2) to obtain sufficiently low pressures in the trapping chamber. Ideally the pressure drops from 10^{-8} mbar in the vacuum system of the beam machine via $\sim10^{-9}$ mbar in the differential pumping chamber to $\sim10^{-10}$ mbar in the trapping chamber. The ion-getter pump currents of both chambers indicate a pressure below 10^{-8} mbar. Both the trapping chamber and differential pumping stage are pumped by 20 l/s ion getter pumps and are equipped with titanium sublimation pumps.

The atom flux is measured in front of the first pumping resistance with an indium tin oxide covered glass plate that can be moved in and out of the beam. From the transverse velocity spread of the atom beam and diameter of the second pumping resistance we estimate that about 80% to 90% of the atom flux from the beam preparation stage will reach the trap center.

B. MOT

We use three laser beams that are retroreflected to make the three pairs of σ^+-σ^- polarized laser beams of the MOT [11]. The radial trapping beams are at 45° with respect to the vertical (see Figs. 1 and 2). The trapping beams are obtained by putting an 18 mm diameter aperture into a 16 mm waist $(1/e^2)$ laser beam. In this way the intensity at the edge of the trapping beams is still 50% of the peak intensity. This ensures efficient capturing of atoms and allows for large MOT cloud diameters. The three trapping laser beams have equal intensity. The total six-beam intensity will be denoted by I_{M}. We also introduce the total six-beam on-resonance saturation parameter $s_{\mathrm{M}}=I_{\mathrm{M}}/I_{\mathrm{sat}}$. The MOT is operated on the $\mathrm{Ne}(3s)\,^3P_2\leftrightarrow\mathrm{Ne}(3p)\,^3D_3$ cycling transition at 640.2 nm, for which the natural linewidth $\Gamma=2\pi\times8.2\times10^6$ rad/s and $I_{\mathrm{sat}}=4.08$ mW/cm^2 for circularly polarized light. The detuning from resonance will be denoted as Δ_{M}. The trapping light can be switched on and off within 2 ms with a mechanical shutter.

The MOT quadrupole field is produced by anti-Helmholz coils made of 4 mm diameter hollow copper tubing. Each coil consists of 24 turns: three layers of eight turns each. The magnetic field gradient of the coil configuration was measured to be $G\equiv\nabla_z B=2\nabla_\rho B=0.33$ G cm^{-1}A^{-1}.

Three sets of Helmholz coils are used for compensating the Earth's magnetic field. These coils can also be used to counteract the displacement of the MOT caused by the additional Zeeman slower laser beam.

C. Zeeman slower

The atoms entering the trapping chamber have an average velocity of 100 m/s which is still too large to be efficiently captured by the MOT. Therefore we included an additional Zeeman slower that reduces the velocity to below 30 m/s. A σ^+-polarized 15 mm diameter laser beam counterpropagates to the atom beam. This beam also crosses the trap region. Two coils on either side of the trap center generate a magnetic field gradient along the atom beam axis. The magnetic fields of the two coils add up in such a way that the field on the upstream side of the trap is eight times larger than on the downstream side, with a field zero at the trap center. The gradient on the left is about 3 G/cm. We operate at a laser intensity $I_{\mathrm{Z}}=0.8$ mW/cm^2 and detuning $\Delta_{\mathrm{Z}}=-6.7\Gamma$.

D. Laser setup

Two dye lasers are used to run the complete setup. One is used for the neon beam preparation, which also supplies the extra Zeeman slower beam and the absorption imaging probe beam. The second laser is completely dedicated to operation of the MOT.

The dye lasers are frequency stabilized to the $(3s)\,^3P_2\leftrightarrow(3p)\,^3D_3$ transition at 640.2 nm using saturated absorption spectroscopy. The linewidth of the lasers is below 1 MHz as determined from measuring the beat node between them. Detuning from the atomic resonance is achieved by Zeeman shifting the saturated absorption line by applying an external magnetic field to the gas discharge cell.

III. MODEL FOR A SEVEN-BEAM MAGNETO-OPTICAL TRAP

A. Trap population

For any atom trap the steady-state number of atoms that can be trapped is a balance between the loading rate and all possible loss processes. In the case of losses due to background gas collisions and two-body intratrap collisions this balance is governed by the differential equation

$$\frac{dN(t)}{dt}=R-\frac{N(t)}{\tau}-\beta\int n^2(\mathbf{r},t)d^3r \tag{1}$$

for the number of atoms $N(t)$ in the trap. Here, R is the loading rate, τ the time constant for density independent losses, β the loss coefficient for intratrap collisions, and $n(\mathbf{r},t)$ the density distribution.

Generally, the density in metastable atom MOTs is low enough to assume that the spatial distribution is independent of the number of trapped atoms, i.e., $n(\mathbf{r},t)=n(\mathbf{r})f(t)$. Our measurements show that the density distribution is Gaussian and does not depend on the number of atoms in the trap. Hence, by introducing the effective volume $V_{\mathrm{eff}}=8\pi^{3/2}\sigma_x\sigma_y\sigma_z$ [17], with σ_i the rms widths of the distributions in the x,y,z directions, Eq. (1) becomes

$$\frac{dN}{dt}=R-\frac{N(t)}{\tau}-\frac{\beta N^2(t)}{V_{\mathrm{eff}}}. \tag{2}$$

The steady-state number of atoms in the trap calculated from Eq. (2) is

$$N_{\mathrm{st}}=\frac{V_{\mathrm{eff}}}{2\beta\tau}\left[\left(1+\frac{4R\beta\tau^2}{V_{\mathrm{eff}}}\right)^{1/2}-1\right]. \tag{3}$$

Solving Eq. (2) for $N(0)=0$ one finds the time dependence of the number of atoms during loading of the MOT:

$$N(t)=N_{\mathrm{st}}\frac{1-\exp(-t/\tau_0)}{1+(N_{\mathrm{st}}^2\beta/V_{\mathrm{eff}}R)\exp(-t/\tau_0)}, \tag{4}$$

with

$$\tau_0=\frac{\tau}{(1+4\beta R\tau^2/V_{\mathrm{eff}})^{1/2}}. \tag{5}$$

After switching off the atom beam from which the trap is loaded the number of atoms decreases according to

$$N(t)=\frac{N_{\mathrm{st}}\exp(-t/\tau)}{1+(\beta N_{\mathrm{st}}\tau/V_{\mathrm{eff}})[1-\exp(-t/\tau)]}. \tag{6}$$

For the values of β and the density obtained in our trap of 5×10^{-10} cm^3/s and 10^{10} atoms/cm^3, respectively, the lifetime determined by the intratrap collisions is $1/(\beta n)=0.2$ s. This is much shorter than the lifetime resulting from background gas collisions, which is on the order of 3 s. This means that in order to simplify the analysis of our MOT we can neglect the N/τ term in Eq. (2) with respect to the $\beta N^2/V_{\mathrm{eff}}$ term. The steady-state number of atoms then becomes

$$N_{\mathrm{st}}\simeq(RV_{\mathrm{eff}}/\beta)^{1/2}. \tag{7}$$

From Eq. (7) the importance of the volume of the trap in determining the number of trapped atoms is immediately clear. A large volume trap keeps the density and consequently the two-body collision rate low such that a steady state is reached with a larger number of atoms in the trap.

B. Doppler model

In the following we develop a simple two-level atom model for the dependence of the volume of trapped atoms on the trap parameters. The size of the atom cloud is determined by the equipartion of kinetic and potential energy of the atoms, resulting in a volume given by

$$V=(2\pi k_BT)^{3/2}(\kappa_\rho^2\kappa_z)^{-1/2}, \tag{8}$$

where T is the temperature of the atoms, and κ_ρ and κ_z are the radial and axial spring constants of the trap, respectively. Note that $V_{\mathrm{eff}}=2\sqrt{2}V$. We assume that the temperature is given by the Doppler cooling limit at a given detuning [18]. As the data in Sec. V A show, this is a valid assumption for our MOT. The spring constant is taken to be the derivative of the photon scattering force of a two-level atom [18]. One then arrives at

$$V=V_0\left[\left(2\delta'+\frac{1}{2\delta'}\right)\frac{(1+s_{\mathrm{M}}/6+4\delta'^2)^2}{\delta'(s_{\mathrm{M}}/6)(G/G_0)}\right]^{3/2}, \tag{9}$$

with

$$V_0=\frac{\pi^{3/2}}{32}\left[\frac{\hbar\Gamma}{k_L\mu_BG_0}\right]^{3/2}, \tag{10}$$

where $G_0=10$ G/cm in the strong direction, k_L is the wave number of the laser light, and $\delta'=\Delta_{\mathrm{M}}/\Gamma$. We have assumed equal intensities in all MOT laser beams. The value of $V_0=2.5\times10^{-9}$ cm^3.

Combining Eq. (7) with Eq. (9) shows that the detuning dependence $V\propto\delta'^6$ for $\delta'\gg1$ will strongly determine how many atoms can be loaded into the MOT at a given Δ_{M}. The ratio R/β is expected not to depend so strongly on Δ_{M} because R and β are likely to scale in the same direction, making the ratio weakly dependent on the specific values of I_{M} and Δ_{M} (see Sec. VII). According to this simple model the number of atoms in the MOT is increased for large detunings and small intensities.

C. Trapping potential: Geometric trap loss

The model states that the number of atoms is fully determined by the volume of the atom cloud. However, the increase of the volume cannot continue forever: for a certain detuning the edge of the atom cloud will shift outside the trapping laser beams. The volume, and therefore the number

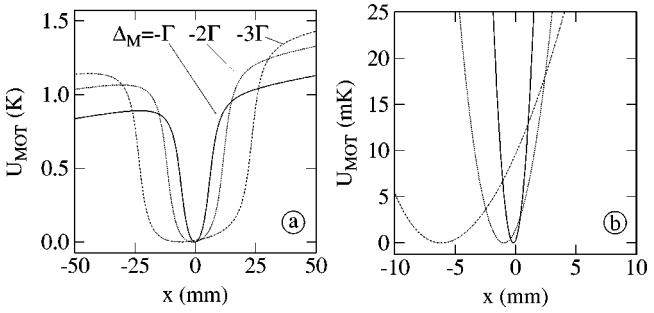

FIG. 3. The full confining potential of the MOT (a) and close-up (b) of the deepest point of the potential for three different detunings of the trapping light. The minimum of the potentials is fixed to 0 K. Trapping conditions are $G=10$ G/cm and $s_M=0.6$.

of trapped atoms, will then no longer increase. In addition, the Zeeman slower beam overlaps with the MOT and consequently pushes the atom cloud out of the center of the trapping beams. This causes the edge of the cloud to shift outside the laser beams at even smaller cloud diameters, which leads to an extra reduction of the volume.

The dependence of the cloud diameter on detuning is given by the Doppler model. The shift of the cloud can be calculated by adding the radiation force of the slower beam to that of the MOT laser beams, where we restrict ourselves to the forces directed along the x axis. The integral of the total force is then an effective trapping potential. A tilted trapping potential is the result as illustrated in Fig. 3, where the potential for different detunings of the MOT beams and fixed intensity is shown. The intensity and detuning of the slower light are fixed at our experimental operating values. The depth of the potential is of the order of 1 K, much more than the expected cloud temperature of 1 mK. If we assume that the atom cloud is centered at the position of the potential minimum it is clear that it will shift when Δ_M is changed. The cloud shifts because the MOT radiation forces become weaker when Δ_M is increased whereas the radiation force from the slower light is fixed because its intensity and detuning are fixed. We can calculate the shift of the deepest point x_0 of the potential for different trapping conditions. Figure 4(a) shows this shift for a number of MOT light intensities.

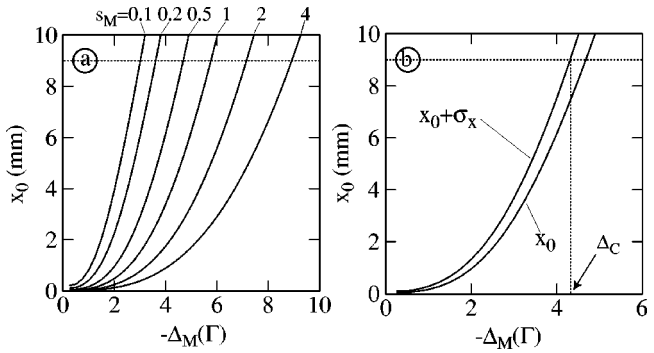

FIG. 4. (a) Shift x_0 of the trap center as a function of Δ_M for different values of s_M and $G=10$ G/cm. In (b) the shift of the edge of the atom cloud $x_0+\sigma_x$ is shown as a function of Δ_M for $s_M=0.5$.

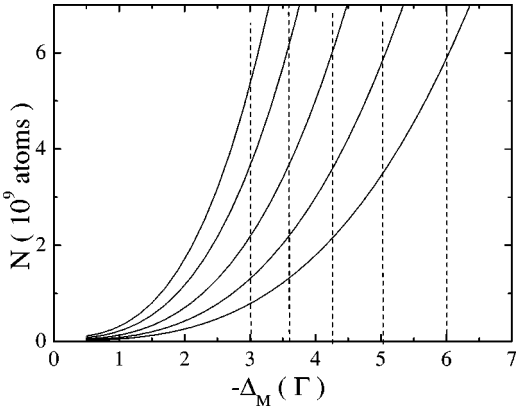

FIG. 5. Calculated number of trapped atoms (solid curves) as a function of the detuning of the trapping beams for $G=10$ G/cm and different MOT light intensities. From left to right $s_M=0.3,0.5,1.0,2.0$, and 4.0. The critical detuning Δ_C is indicated by vertical dashed lines.

The displacement is seen to easily become as large as 10 mm, which is larger than the radius of the MOT laser beams. For small s_M the minimum in the potential shifts away from the trapping center faster than for large s_M, i.e., the curves in Fig. 4 are steeper for small s_M.

In order to know what the limiting volume of the cloud will be we need to add the radius of the cloud to the shift. This results in a critical detuning Δ_C where the edge of the cloud starts to shift outside the laser beams. This is illustrated in Fig. 4(b). For $\Delta_M>\Delta_C$ the cloud diameter starts to shrink again because the cloud radius is determined by the distance between the potential minimum and the edge of the MOT laser beams. The MOT becomes leaky at the edges and due to the strongly reduced volume the number of atoms also decreases strongly. We call this *geometric loss*.

We can now estimate how many atoms can be loaded into our MOT. We insert the effective volume calculated from Eq. (9) into Eq. (7) and assume $R=2.4\times10^{10}$ s^{-1} (100% capturing efficiency) and the theoretical value $\beta=8\times10^{-10}$ cm^3/s [19]. For the time being we assume R and β to be independent of Δ_M, I_M, and G. This is not fully correct, as will be discussed later, but allowed because we expect the detuning dependence of the volume to dominate completely. Figure 5 shows the result for a number of trapping conditions. The number of trapped atoms strongly increases with increased detuning as expected. We assume that the maximum number of atoms N_{max} will be reached at $\Delta_M=\Delta_C$. Figure 5 shows that about 6×10^9 atoms can be loaded for a large range of MOT parameters.

IV. DIAGNOSTICS

Our setup is equipped with a number of diagnostic tools to measure number, size, and temperature of the atom cloud in the MOT. This section gives an overview of the techniques used to obtain the data presented in this paper.

A. Fluorescence

The fluorescence from the cloud of atoms held by the MOT is used to determine the total number and size of the

cloud. The geometry of the detection system is shown in Fig. 1. The use of a beam splitter enables a simultaneous measurement of the total fluorescence and the imaging of the cloud onto a charge-coupled device (CCD) camera.

Townsend *et al.* [20] found empirically that the total emitted fluorescence power of a cloud of N cesium atoms held in their MOT is given by

$$P_{\text{fluor}} = N\hbar\omega\frac{\Gamma}{2}\left[\frac{Cs_{\text{M}}}{1+Cs_{\text{M}}+4\delta'^2}\right], \tag{11}$$

where the coefficient $C=0.7$ takes into account that the atoms are multilevel atoms moving in the spatially changing light polarization of the six MOT laser beams. For the helium MOT discussed in [17], the value of C turned out to be slightly smaller than the averaged Clebsch-Gordan coefficients. The average of the squares of the Clebsch-Gordan coefficients of the neon cooling transition is 0.46. We adopt the value $C=0.7$ for calculating the number of atoms in our trap. In this way we are more likely to underestimate the number of atoms than vice versa.

During the measurement of the number of atoms in the MOT the slower beam is also present, which results in additional fluorescence from the atoms. We correct our numbers for this effect, again using Eq. (11). Furthermore, due to the large cloud diameters in our MOT the magnetic field gradient causes the atoms at the edge of the cloud to Zeeman-shift closer to resonance. This effect on the fluorescence amounts to about 20% for the largest clouds and is also corrected for in the presented data. When the uncertainty in the phenomenological parameter C is neglected, the relative uncertainty in the number of trapped atoms is about 10%. The largest contribution to this uncertainty is produced by the 1 MHz, i.e., 0.13Γ, uncertainty in the frequency of both trapping and slower lasers.

The volume of the atom cloud can be measured by analyzing fluorescence images taken with a CCD camera, positioned below the trapping chamber (Fig. 1). By fitting the intensity profile of the CCD frames with Gaussians the rms width in the x and z directions can be determined. The images are well described by Gaussians. In order to calculate V_{eff} from the measured sizes we assume that the width in the y direction is equal to that in the x direction. This assumption is based on the radial symmetry of the MOT magnetic quadrupole field. The relative uncertainty in the measured volume is approximately 12%, and is determined by the uncertainty in the Gaussian fits and the uncertainty in the conversion from pixels to real sizes.

B. Absorption imaging

In addition to the fluorescence imaging we apply absorption imaging to measure the size, number, and temperature of the atom cloud in the MOT. We image the atoms while the MOT is running in a steady state. The laser beam used for this is spatially filtered by a single-mode optical fiber. The laser beam has a Gaussian waist of 40 mm which is apertured down to a diameter of 20 mm in order to avoid reflection and scattering at the edges of the vacuum windows. This imaging beam is directed along the z axis and imaged onto a CCD camera. The intensity of the probe beam is $0.03\times I_{\text{sat}}$ and the exposure time 30 μs, small enough not to influence the trap population. The detuning is adjusted such that the optical density is about unity.

Using the absorption images we can also measure the size of the atom cloud in the y direction and have a consistency check of the cloud size in the x direction. Integrating the two-dimensional optical density profile over the complete image gives us a consistency check on the total number of atoms as compared to the total measured fluorescence. We find that the absorption images give a total atom number that is about 20% to 50% higher than obtained from the fluorescence measurement.

The absorption imaging technique is also used to measure the temperature of the atoms in the MOT. After switching off the MOT light and magnetic fields, the atom cloud expands ballistically. The radial velocity distribution of the atom cloud is inferred from the radial expansion rate.

C. Metastable atom time of flight

Working with metastable atoms gives us an extra measurement tool. As indicated in Fig. 1 we have installed a channeltron 40 mm *above* the center of the MOT, which allows us to detect UV photons, metastable atoms, and ions originating from the trap. In front of the entrance of the channeltron (type Galileo 4039) a grid is placed which can be put on a positive voltage to measure only metastable atoms and UV photons, or on a negative voltage to also detect ions. We use the metastable atom signal to measure the temperature. This is done by measuring the time-of-flight distribution of the detector current after the MOT light is switched off and the cloud expands ballistically. Assuming that the velocity distribution of the trapped atoms satisfies a Maxwell-Boltzmann distribution, the channeltron signal $I(t)$ is given by

$$I(t)\propto\frac{(v_{y,0}-gt)}{t^3}\exp\left(-\frac{v_{y,0}^2}{2\sigma_y^2}\right). \tag{12}$$

Here, $v_{y,0}$ is the initial velocity of the atoms hitting the detector at time t,

$$v_{y,0}=\frac{y_d+\frac{1}{2}gt^2}{t}, \tag{13}$$

with $y_d=40$ mm the distance from the channeltron to the trapping center, and g the acceleration caused by gravity. The temperature is calculated from the vertical rms velocity spread σ_y.

V. MODEL VERSUS EXPERIMENT

The Doppler model described in Sec. III predicts two typical behaviors. As a function of the laser detuning the volume of the cloud of atoms increases strongly and its center shifts along the axis of the Zeeman slower beam. Both

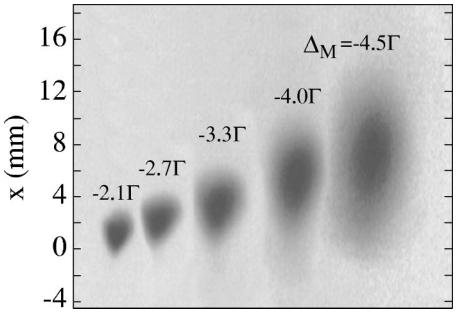

FIG. 6. *In situ* CCD images of clouds of atoms trapped in the MOT for different values of Δ_M, and $s_M=0.4$ and $G=23$ G/cm.

effects are demonstrated in Fig. 6, which shows fluorescence images of the cloud *in situ*, i.e., taken while the MOT is switched on. From the image taken at -4.5Γ it is clear that the effective volume of our MOT clouds can be as huge as 1 cm^3. This is three orders of magnitude larger than a typical alkali-metal MOT. In the following we will look into some MOT properties in more detail and present data that support the Doppler model.

A. Temperature

One of the assumptions in our model is that the temperature of the atoms is close to the Doppler limit. To check this assumption and to characterize our MOT we measured the temperature for a number of MOT conditions.

A systematic measurement of the temperature was done with the metastable atom time-of-flight (TOF) technique described earlier. Two of the measured time traces are shown in Fig. 7, for different MOT parameters. From the TOF signals shown in Fig. 7 it is clear that the temperature of the cloud increases for larger laser detunings as expected from the Doppler cooling model [18]. Curve fits of the expected signal shape are also shown in Fig. 7 by the dashed curves. From these the temperature of the atom cloud was determined for different laser detunings. The results are shown in Fig. 8. The temperature of the cloud is close to the Doppler temperature, which is indicated by the solid curve. Around the critical detuning, the temperature starts to increase, probably due to the geometric loss process or through a larger

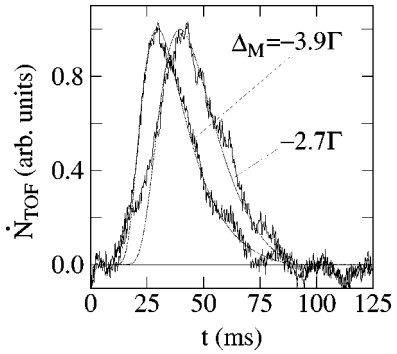

FIG. 7. Metastable atom TOF signals for a MOT operated with laser beam intensity $s_M=0.8$ for two detunings. The curves are fits to the data of the model described in the text.

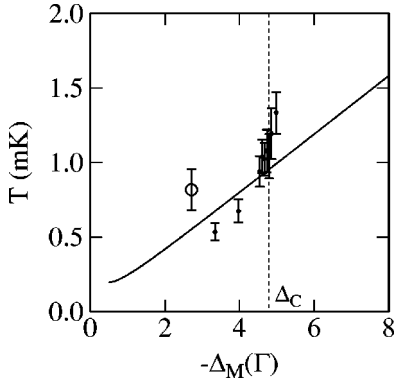

FIG. 8. Temperature of the MOT atoms as a function of detuning, obtained from metastable atom TOF (●) at $s_M=0.8$ and absorption imaging (○) for $s_M=1.1$ and $G=7.6$ G/cm.

heating influence of the slower laser beam.

As a consistency check we applied absorption imaging to a MOT at relatively high intensity $s_M=1.1$, and $\Delta_M=-2.7\Gamma$ and $G=7.6$ G/cm. For these parameters the cloud is relatively dense and can still be imaged well after 7 ms of expansion. The detuning of the probe beam was taken as $\Delta_{probe}=-\Gamma/2$. From the rate of expansion in the horizontal and vertical directions we find a temperature of $T_x=0.78\pm0.15$ mK and $T_y=0.85\pm0.13$ mK, respectively. This is slightly higher than the expected Doppler temperature at this trapping condition, which is 0.55 mK. The result is in agreement with the temperature determined from the metastable TOF signals.

We conclude that the temperature of the atom cloud is close to the Doppler temperature and scales accordingly with detuning. This validates our assumption in deriving the volume of the cloud in terms of a Doppler model (Sec. III).

B. Volume as a function of detuning

The strong detuning dependence of the volume is illustrated by the data shown in Fig. 9(a). Data are shown taken for different values of s_M at a fixed value $G=23$ G/cm. On varying Δ_M from -2Γ to -5Γ, the volume typically increases by a factor of 20 to 50, depending on s_M. At higher intensities the volume does not increase as strongly. Note that V can become as large as 0.5 cm^3 resulting in V_{eff}

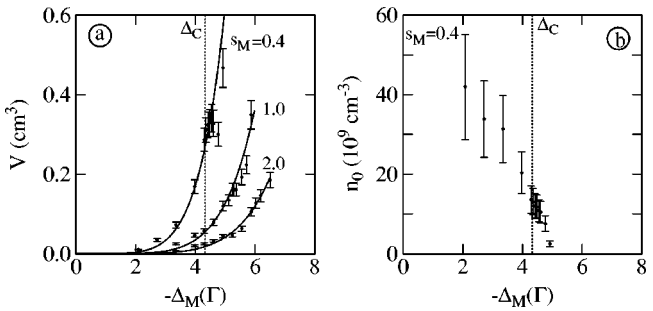

FIG. 9. Volume (a) and density (b) of the cloud of atoms in the MOT as a function of the MOT laser detuning for different s_M values and $G=23$ G/cm. The critical detuning is indicated for the $S_M=0.4$ trapping condition (dotted line).

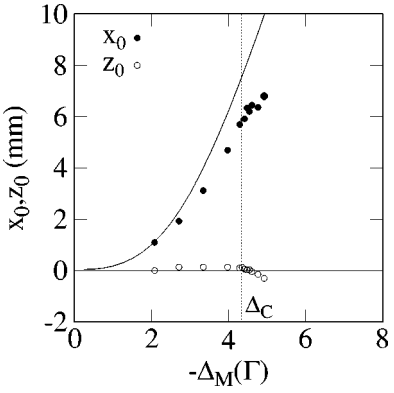

FIG. 10. Radial x_0 (●) and axial z_0 (○) displacement of the measured trap center as a function of Δ_M for $s_M=0.4$ and $G=23$ G/cm. The solid curves show the shifts predicted by the Doppler model (Sec. III C).

$=1.4$ cm^3. It is at these large volumes that the largest number of atoms is trapped. At the critical detuning the number of trapped atoms was $N_{max}=6\times10^9$ for the $s_M=0.4$ data set.

From the volume of the cloud and the number of atoms in the cloud we can estimate the central density $n_0=N/V$. With V increasing rapidly as a function of Δ_M the density remains low. This is illustrated by the data in Fig. 9(b), where the central density n_0 is plotted as a function of Δ_M. At the detuning where the largest samples are trapped, i.e., at the critical Δ_C, the density is about 1×10^{10} atoms/cm^3.

Comparing the data with Eq. (9) we find that the measured volumes are much larger than the model predicts. However, by using V_0 as a single fit (scaling) parameter we obtain the solid curves shown in Fig. 9(a). Clearly, the model predicts the correct dependence of the volume on detuning. Moreover, data sets taken for different intensities ($s_M=0.4$ to 2.0) and magnetic field gradients (10 to 23 G/cm) all result in the same value of $V_0^{fit}=(1.1\pm0.2)\times10^{-8}$ cm^3. Here the uncertainty refers to the spread of the fits.

The discrepancy between V_0 and V_0^{fit} can be explained partly from the fact that the model is based on the Doppler force for a simple two-level atom. In reality the force becomes smaller because the Clebsch-Gordan coefficients of the different sublevels have to be included. If we take care of this by substituting $0.46s_M$ for s_M we find $V_0=0.8\times10^{-8}$ cm^3, close to the fitted value. We checked that the volume is independent of the number of atoms in the trap. This was found by decreasing the loading rate and measuring the volume again.

We find that the detuning dependence of the volume of the cloud of atoms in our MOT is described qualitatively very well and quantitatively quite reasonably by the Doppler model described in Sec. III.

C. MOT displacement

From fluorescence images like that shown in Fig. 6 the displacement of the atom cloud can be inferred. Figure 10 shows the coordinates of the cloud center (x_0,z_0) as a function of Δ_M for the $s_M=0.4$ data set of Fig. 9(a). We see that, going from $\Delta_M=-2\Gamma$ to -5Γ, the cloud center moves 6 mm in the radial (x) direction, while in the axial direction (z) the cloud stays more or less fixed as expected. The solid curve in the figure indicates the radial shift calculated with the model of Sec. III C. We see that the displacement is described rather well by the Doppler model.

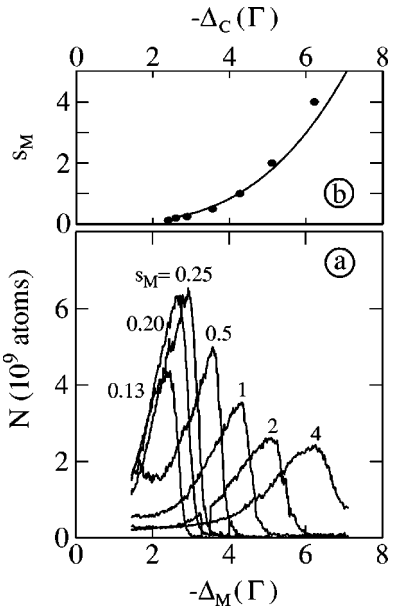

FIG. 11. (a) Number of trapped atoms N as a function of Δ_M for different s_M and fixed $G=10$ G/cm. (b) Measured Δ_C as a function s_M (●), determined from the data in (a). The solid curve in (b) is derived from the Doppler model discussed in the text.

VI. MAXIMIZING TRAP POPULATION

To optimize the number of atoms in our MOT we measured the steady-state population for a large range of MOT parameters. Throughout this section the atom number is determined from the total fluorescence as described in Sec. IV A.

Figure 11(a) shows the number of trapped atoms as a function of the laser detuning for different laser beam intensities and a fixed magnetic field gradient. For each intensity the number of trapped atoms increases until the critical detuning Δ_C, beyond which the number of atoms suddenly decreases. For the measured critical detuning we take the detuning at which the measured amount of trapped atoms is maximum, i.e., N_{max}. We see that this critical detuning increases for increasing intensities and simultaneously N_{max} decreases. The corresponding measured critical detuning is compared to the Doppler model in Fig. 11(b). We observe good agreement with the geometric loss model.

For higher laser beam intensities the drop in the amount of atoms beyond the critical detuning is more gradual, as can be seen in Fig. 11(a). This is also in agreement with the model as can be inferred from Fig. 4(a). The curves predicting the shift of the center of the cloud are less steep for higher laser intensities. We find that the number of atoms in the MOT is maximized for low intensity, $s_M=0.25$ and $\Delta_M\approx-3\Gamma$ for $G=10$ G/cm.

To find the optimum magnetic field gradient we keep the

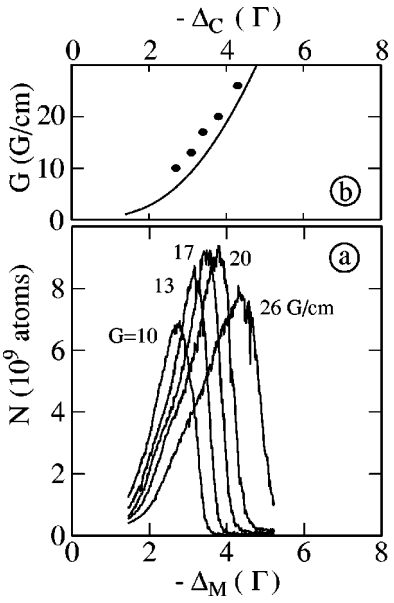

FIG. 12. (a) Number of atoms N in the MOT as a function of the laser detuning Δ_M, for different magnetic field gradients G for $s_M = 0.4$. In (b) measured (●) and calculated (solid curve) critical detuning as a function of the magnetic field gradient G.

intensity fixed at $s_M = 0.4$ and measure the number of atoms again as a function of Δ_M for different values of G. The resulting data are shown in Fig. 12(a). We find that for increasing G values N_{max} increases and Δ_C shifts to larger detunings. An optimum is reached at $G = 20$ G/cm, beyond which N_{max} decreases again. We find a maximum number of ^{20}Ne atoms of $N_{max} = 9 \times 10^9$ for $s_M = 0.4$, $\Delta_M = -3.8\Gamma$, and $G = 20$ G/cm.

As can be inferred from Fig. 12(b) the shift of Δ_C is in agreement with the model discussed in Sec. III C. Larger gradients allow for larger Δ_C. This also means that despite the inverse scaling of V with $G^{3/2}$ traps with larger volumes can be obtained at larger values of G. The decrease of N_{max} for large G values may be caused by a deterioration of the Doppler cooling and trapping forces due to strong magnetic fields, especially at the edges of the cloud [21,22].

A point of concern is the fact that the model described in Sec. III predicts that N_{max} hardly depends on intensity, whereas our data show a strong dependence (see Fig. 11). This difference can be explained by the fact that the assumption of constant R and β being is too strong a simplification of reality. As we will show in the next section, both depend on intensity and detuning in a way that to a large extent explains the discrepancy.

VII. TRAP DYNAMICS

The steady-state number of trapped atoms as optimized in the previous section is not the only parameter that characterizes the trap. The loading efficiency and lifetime are also important. The two-body loss rate β due to ionizing collisions is of particular interest to explain the intensity dependence of N_{max} and for future work toward BEC. These quantities can be inferred by measuring the number of atoms in the trap as a function of time, during loading as well as after the loading is stopped. Figure 13 shows an example of such a measurement. The number of atoms increases as the loading is started, reaches a steady state after about a second, and decreases again when the atom beam is switched off. The Zeeman beam is kept on during the whole measurement, i.e., we retain a seven-beam MOT configuration.

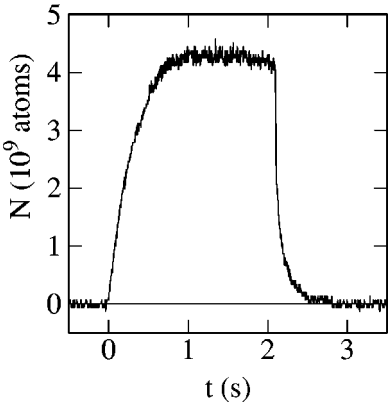

FIG. 13. Experimental loading and decay curve of the trap. At $t = 0$ the loading of the trap is started, i.e., the atomic beam is switched on; at $t = 2.1$ s the loading is stopped. Trapping conditions are $\Delta_M = -4.4\Gamma$, $s_M = 0.4$, and $G = 23$ G/cm.

We determine R, β, and τ for a number of trapping conditions from time traces as shown in Fig. 13. This is done by curve fitting Eq. (4) and Eq. (6) to the rising and falling edge of the time trace, respectively. In a self-consistent way both sides are fitted at the same time with the same parameters. We find an exponential lifetime of $\tau = 3 \pm 1$ s throughout the range of MOT parameters where we operated our MOT.

A. Loading efficiency

We find that at the optimum conditions the loading rate is about 90% of the atom beam flux, consistent with the loss of atoms due to the pumping resistance. This means that the full 100% of the atoms reaching the center of the trapping chamber can be captured for the optimum loading parameters. The precise value of the loading rate is seen to be rather sensitive to the alignment of the MOT laser beams and slower beam, which causes day to day variations. This makes it hard to give a detailed quantitative picture. However, qualitatively some general trends are clearly visible in the data. At a fixed detuning the loading rate increases nearly linearly with increasing intensity and tends to level off for $s_M > 1$. When the intensity is kept constant the loading rate decreases with increasing detuning, for the range of detunings used throughout this paper.

B. Trap lifetime

As mentioned in Sec. III A the lifetime of the trap is dominated by two-body intratrap collisions, i.e., Penning ionization. In that section we characterized this loss with the coefficient β. For simplicity of the model we assumed β to be independent of I_M and Δ_M. However, although most atoms in the trap are in the "ground" (g) state $^3P_2$ a small

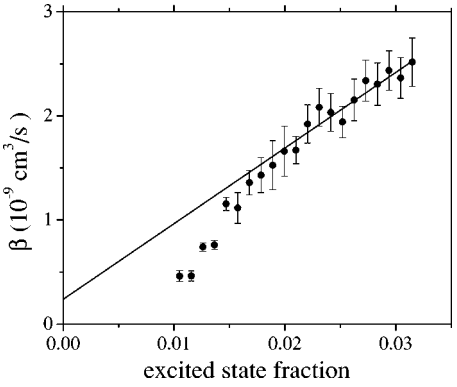

FIG. 14. Measured β (●) as a function of the excited state fraction. The solid line is a linear fit to the data for $\Pi_e > 0.02$.

fraction is excited to the "excited" (e) state $^3D_3$ due to optical pumping induced by the trapping light and Zeeman slower light. This results in three possible types of collision between two atoms in the MOT: g-g, g-e, and e-e. Furthermore, the cross sections for ionization of the three types of collision differ. Hence, β is a function of the populations Π_g and Π_e of the "ground" and "excited" states, respectively. The simplest model to describe this can be written as

$$\beta = \Pi_g^2 \mathcal{K}_{gg} + 2\Pi_g \Pi_e \mathcal{K}_{ge} + \Pi_e^2 \mathcal{K}_{ee}, \tag{14}$$

with $\mathcal{K}_{ij}$ the rate coefficients for i-j collisions. Experiments with metastable helium atoms [15–17,23] show that $\mathcal{K}_{ge}$ can be two orders of magnitude larger than $\mathcal{K}_{gg}$ and that $\mathcal{K}_{ee}$ can be neglected [23]. Mastwijk *et al.* [14], however, report a $\mathcal{K}_{ge}$ which is only a factor of 20 larger then $\mathcal{K}_{gg}$, for metastable helium. To our knowledge, no experimental results have been reported for metastable neon atoms so far.

A detailed study of the light assisted collisions in our neon MOT is beyond the scope of this paper. Here we restrict ourselves to describing the general trends in order to explain the scaling of N_{max} with I_M. To this end we measured β as a function of the intensity for a fixed detuning of -3Γ. The result is shown in Fig. 14. For comparison with Eq. (14) we have plotted β as a function of the excited state fraction

$$\Pi_e = \frac{s_M/2}{1 + s_M + 4(\Delta_M/\Gamma)^2} + \frac{s_Z/2}{1 + s_Z + 4(\Delta_Z/\Gamma)^2}, \tag{15}$$

taking into account the slower beam as well. The data in Fig. 14 indeed show a strong dependence of β on intensity. By measuring the ion production rate $R_{ion} \propto \beta N^2/V_{eff}$ with the channeltron this increase of β could be confirmed.

For the data set shown in Fig. 14 the smallest measured value of β is $(4 \pm 1) \times 10^{-10}$ cm^3/s. In general we find that the observed values of β never drop down to the zero intensity value of 8×10^{-11} cm^3/s predicted by theory [19], for detunings ranging from -2Γ to -6Γ. Our lowest intensity data for different detunings can be summarized by stating that $\mathcal{K}_{gg} = (5 \pm 3) \times 10^{-10}$ cm^3/s. This large value could point to an underestimation of the density in our MOT. The data in Fig. 14 show another typical behavior. Below a given intensity β drops faster than expected from Eq. (14) when the intensity is decreased. This is illustrated in Fig. 14 where we show the curve of Eq. (14) fitted to the $\Pi_e > 0.02$ data points. The deviation at low intensities may be explained by the fact that the MOT cloud changes its shape. Because of this we may underestimate the volume of the cloud which is calculated from σ_x and σ_z only, obtained from the fluorescence images. Nevertheless, the high intensity data do not suffer from this effect. The fit of Eq. (14) to the data in Fig. 14 gives $\mathcal{K}_{ge} = (3.5 \pm 1.0) \times 10^{-8}$ cm^3/s. We plan to investigate light assisted collisions in our MOT in more detail in the future.

We now come back to the fact that the measured N_{max} values shown in Fig. 11 decrease by a factor of 3 with increasing intensity, whereas according to the model N_{max} is nearly independent of intensity. The scatter in the loading rate data does not allow for a quantitative explanation of this discrepancy. The data for β show much less scatter. To estimate what the influence of β is on N_{max}, we assume that Eq. (14) gives a reasonable description of the intensity and detuning dependence of β when we take Eq. (15) to calculate the excited state fraction. The values of $\mathcal{K}_{gg}$ and $\mathcal{K}_{ge}$ are determined from the data in Fig. 14. We calculated the number of atoms in the MOT again for constant R but now inserting the detuning and intensity dependent β. The result is that N_{max} decreases by a factor of 1.8 when the intensity is increased from $s_M = 0.4$ to $s_M = 4.0$. So part of the decrease of N_{max} can be explained by the intensity and detuning dependence of β. The remaining decrease of N_{max} found in the data must then be attributed to intensity and detuning dependencies of R.

VIII. PROSPECTS FOR BOSE-EINSTEIN CONDENSATION

A MOT containing close to 10^{10} atoms is a good starting point on the road to BEC [7]. Moreover, by locking the lasers to the resonance frequency of the ^{22}Ne isotope, we trapped 3×10^9 atoms of that isotope for the same MOT parameters. This gives us the opportunity to switch to the less abundant isotope if the scattering length turns out to be too small or even negative.

In addition to the bosonic isotopes the fermionic isotope ^{21}Ne is also available in our setup. By scanning the frequency of the laser that is used for preparing the bright neon beam we were also able to generate a ^{21}Ne beam with 7×10^7 atoms/s. Taking into account that a repumper was not used in this case a flux of over 10^8 atoms/s seems feasible [12]. This holds the promise of making large MOTs of the fermionic isotope ^{21}Ne also. A spin polarized sample of fermions would have an even smaller Penning ionization rate due to Pauli blocking of S-wave collisions.

The large diameter of the cloud of atoms in the MOT has the advantage that the relative alignment of the MOT and magnetic trap centers during the transfer from one trap to the other is not very critical. The clover-leaf magnetic trap that we have installed gives oscillation frequencies of 45 Hz in all three dimensions when the atoms are transferred. With such a shallow trap misalignments of 1 mm are still acceptable. A disadvantage is that the initial density in the magnetic trap will be low. In order to increase the elastic collision rate

to values where evaporative cooling starts to work the trap has to be compressed. We can do this by reducing the bias field to about 1.5 G, which increases the radial oscillation to 350 Hz. In a first attempt we successfully transferred 70% of the atoms from the MOT to the magnetic trap. In between the MOT being switched off and the magnetic trap being switched on we applied a σ^+-polarized laser beam along the z direction to spin polarize the atoms. The transfer efficiency was determined by switching the magnetic trap off after 300 ms and recapturing the atoms in the MOT.

The temperature of the atoms in the MOT was found to be in the Doppler limited regime, i.e., temperatures around 1 mK. For the highest measured density, i.e., 4×10^{10} atoms/cm^3, this corresponds to a phase space density of $n\Lambda^3\simeq10^{-7}$. Before loading the atoms into a magnetic trap we plan a short optical molasses phase to reduce the temperature and increase the phase space density by an order of magnitude.

The lifetime of the MOT due to background gas collisions is presently only 3 s. The reason for this short lifetime is a leaking vacuum window. This lifetime is too short to reach BEC by means of evaporative cooling. Therefore a replacement chamber is currently being built. The new chamber will enable us to reach much better lifetimes, i.e., longer than the 24 s lifetime of the metastable state of the neon atoms.

IX. CONCLUDING REMARKS

In conclusion, we trapped almost 10^{10} metastable ^{20}Ne and 3×10^9 metastable ^{22}Ne atoms in a MOT. This was achieved at low intensity of the trapping beams, i.e., $s_M\simeq0.25$. The optimum trapping field is around $G=20$ G/cm. At the optimum trapping conditions the cloud has a very large volume of about 1 cm^3. The simple Doppler model and the picture of the seven-beam MOT discussed in Sec. III explain the trap charateristics quite well.

The optimum operating conditions differ strongly from those used in metastable helium experiments [4,14–17], where very high intensities [$(100–200)\ I_{sat}$] and large detunings [$(20–30)\Gamma$] are used. Due to the very small natural linewidth $\Gamma_{He*}/2\pi=1.6$ MHz of the laser cooling transition of helium, a different strategy can be chosen where essentially a boxlike potential is created by using a very large detuning in conjunction with a large gradient and subsequently high intensity. Due to the much larger linewidth of the neon transition this strategy would require experimentally unrealistically high laser powers and gradients. Luckily such a strategy is not necessary for metastable neon as the data presented here show. This holds the promise that our strategy may also work for the heavier rare gasses such as Ar, Kr, and Xe.

The fact that the absorption imaging technique systematically gives higher total atom number than the fluorescence technique may mean that we underestimate the number of atoms in the MOT. Also, the rather large value of $\mathcal{K}_{gg}$ points in the direction of underestimating the density. We therefore believe that the value of $\mathcal{K}_{gg}$ presented here sets an upper limit.

ACKNOWLEDGMENTS

We thank M. Kurzanov and E. van Kempen for their help in building parts of the setup. We thank R. de Koning, L. van Mol, and J. van de Ven for their technical assistance. We thank P. van der Straten for helpful discussions during the preparation of this manuscript. This work was financially supported by the ''Stichting voor Fundamenteel Onderzoek der Materie (FOM).''

[1] M.H. Anderson, J.R. Ensher, M.R. Matthews, C.E. Wieman, and E.A. Cornell, Science **269**, 198 (1995); K.B. Davis, M.-O. Mewes, M.R. Andrews, N.J. van Druten, D.S. Durfee, D.M. Kurn, and W. Ketterle, Phys. Rev. Lett. **75**, 3969 (1995); C.C. Bradley, C.A. Sackett, J.J. Tollett, and R.G. Hulet, *ibid.* **75**, 1687 (1995).

[2] W. Rooijakkers, W. Hogervorst, and W. Vassen, Opt. Commun. **135**, 149 (1997).

[3] S. Nowak, A. Browaeys, J. Poupard, A. Robert, D. Boiron, C. Westbrook, and A. Aspect, Appl. Phys. B: Lasers Opt. **70**, 455 (2000).

[4] F. Pereira Dos Santos, F. Perales, J. leonard, A. Sinatra, J. Wang, F.S. Pavone, E. Rasel, C.S. Unnikrishnan, and M. Leduc, Eur. Phys. J.: Appl. Phys. **14**, 69 (2001).

[5] M. Zinner, C. Jentsch, G. Birkl, and W. Ertmer (private communication).

[6] G.V. Shlyapnikov, J.T.M. Walraven, U.M. Rahmanov, and M.W. Reynolds, Phys. Rev. Lett. **73**, 3247 (1994).

[7] H.C.W. Beijerinck, E.D.J. Vredenbregt, R.J.W. Stas, M.R. Doery, and J.G.C. Tempelaars, Phys. Rev. A **61**, 023607 (2000).

[8] F. Dalfolvo, S. Giorgini, L.P. Pitaevskii, and S. Stringari, Rev. Mod. Phys. **71**, 463 (1999).

[9] A. Robert, O. Sirjean, A. Browaeys, J. Poupard, S. Nowak, D. Boiron, C.I. Westbrook, and A. Aspect, Science **292**, 461 (2001).

[10] F. Pereira Dos Santos, J. Léonard, Junmin Wang, C.J. Barrelet, F. Perales, E. Rasel, C.S. Unnikrishnan, M. Leduc, and C. Cohen-Tannoudji, Phys. Rev. Lett. **86**, 3459 (2001).

[11] E.L. Raab, M. Prentiss, A. Cable, S. Chu, and D.E. Pritchard, Phys. Rev. Lett. **59**, 2631 (1987).

[12] J.G.C. Tempelaars, R.J.W. Stas, P.G.M. Sebel, H.C.W. Beijerinck, and E.J.D. Vredenbregt (unpublished).

[13] F. Shimizu, K. Shimizu, and H. Takuma, Phys. Rev. A **39**, 2758 (1989).

[14] H.C. Mastwijk, J.W. Thomsen, P. van der Straten, and A. Niehaus, Phys. Rev. Lett. **80**, 5516 (1998).

[15] M. Kumakura and N. Morita, Phys. Rev. Lett. **82**, 2848 (1999).

[16] P.J.J. Tol, N. Herschbach, E.A. Hessels, W. Hogervorst, and W. Vassen, Phys. Rev. A **60**, R761 (1999).

[17] A. Browaeys, J. Poupard, A. Robert, S. Nowak, W. Rooijakkers, E. Arimondo, L. Marcassa, D. Boiron, C.I. Westbrook,

and A. Aspect, Eur. Phys. J. D **8**, 199 (2000).
[18] H.J. Metcalf and P. van der Straten, *Laser Cooling and Trapping* (Springer-Verlag New York, 1999).
[19] M.R. Doery, E.J.D. Vredenbregt, S.S. Op de Beek, H.C.W. Beijerinck, and B.J. Verhaar, Phys. Rev. A **58**, 3673 (1998).
[20] C.G. Townsend, N.H. Edwards, C.J. Cooper, K.P. Zetie, C.J. Foot, A.M. Steane, P. Szriftgiser, H. Perrin, and J. Dalibard, Phys. Rev. A **52**, 1423 (1995).
[21] M. Walhout, J. Dalibard, and S.L. Rolston, J. Opt. Soc. Am. B **9**, 1997 (1992).
[22] J. Werner, H. Wallis, and W. Ertmer, Opt. Commun. **94**, 525 (1992).
[23] F. Bardou, O. Emile, J.-M. Courty, C.I. Westbrook, and A. Aspect, Europhys. Lett. **20**, 681 (1992).